Supplementary Information for Extracting Three-Dimensional Molecular Structure with Multiparticle Covariance and Cumulant Coulomb Explosion Analysis

Chuan Cheng,[†] Yoshiaki Kumagai,[‡] Kiyonobu Nagaya,[¶] Tatsuo Gejo,[§] Michael Burt,[‖] Mark Brouard,[‖] Avijit Duley,[⊥] James Harries,[#] Paul Hockett,[@] Joseph W. McManus,[‖] Russell S. Minns,[△] Subhendu Mondal,[▽] Shigeki Owada,[††] Weronika Razmus,[△] Daniel Rolles,[⊥] Takahiro Sato,[¶¶] Henry Thompson,[△] Anbu Venkatachalam,[⊥] Emily Warne,[‖] Tiffany Walmsley,[‖] Mana Yagi,[§] Philip Bucksbaum,[§§] Felix Allum,[†] and Ruaridh Forbes*[,¶¶,‖‖]

†*PULSE Institute, SLAC National Accelerator Laboratory, Menlo Park, California, 94025, USA*

‡*Department of Applied Physics, Tokyo University of Agriculture and Technology, Tokyo, 184-8588, Japan*

¶*Department of Physics, Kyoto University, Kyoto, 606-8502, Japan*

§*Graduate School of Material Science, University of Hyogo, Kouto 3-2-1, Kamigori-cho, Ako-gun, Hyogo 678-1297, Japan*

‖*Chemistry Research Laboratory, Department of Chemistry, University of Oxford, Oxford, OX1 3TA, UK*

⊥*J.R. Macdonald Laboratory, Department of Physics, Kansas State University, Manhattan, Kansas, 66506, USA*

#*QST, SPring-8, Kouto 1-1-1, Sayo, Hyogo, 679-5148, Japan*

@*National Research Council of Canada, Ottawa, ON K1A 0R6, Canada*

△*School of Chemistry, University of Southampton, Highfield, Southampton, SO17 1BJ, UK*

▽*Haldia Institute of Technology, Haldia, 721657, India*

††*RIKEN SPring-8 Center, Sayo, Hyogo, 679-5148, Japan*

‡‡*Japan Synchrotron Radiation Research Institute, Hyogo, 679-5198, Japan*

¶¶*Linac Coherent Light Source, SLAC National Accelerator Laboratory, Menlo Park, CA 94025, USA*

§§*PULSE Institute, SLAC National Accelerator Laboratory, Menlo Park, California, 94025, USA*

‖‖*Department of Chemistry and Department of Physics, University of California, Davis, CA 95616, USA*

E-mail: ruforbes@ucdavis.edu

Influence of the 800 nm laser

The experimental data were recorded in a two-color pump-probe experiment, in which the delay of a few-cycle near-infrared (NIR) laser pulse relative to the X-ray pulse was scanned. The data presented in the current work was averaged over all pump-probe delays to improve statistics. The primary effect of the NIR laser pulse was to initiate single ionization, which was observed to lead to a significant amount of dissociative ionization into $C_4H_7^+$ + I. This dissociative ionization process could then be probed with the intense soft X-ray pulse, primarily through the observation of a (weak, $\sim$ few percent of total signal) delay-dependent feature in the I^{2+}, which results from a delay-dependent Coulombic repulsion against the $C_4H_7^+$ following I 4d ionization of the I atoms produced in this dissociative ionization. Analysis of this time-resolved data will be presented in another publication. As the dissociative ionization process should effectively prevent the molecule from reaching the very high charge-states required for complete Coulomb explosion (as, following dissociation, I 4d ionizations will no longer result in charges being deposited on the alkyl chain), we do not expect this to interfere with the ground-state X-ray Coulomb explosion signals considered in the present work.

In order to verify that this additional laser pulse has a very limited effect on the presented results, we consider the delay-dependent momentum distribution of I^+, I^{2+}, C^+ and C^{2+} ions (the primary ions considered in the analysis presented in the main text). Clear delay-dependent effects are observed only in the I^{2+} ion — in the form of the aforementioned "Coulomb curve" feature arising from NIR-induced dissociative ionization, prior to probing at the iodine. This leads to ions with lower momentum than those produced by Coulomb explosion of ground-state molecules. To confirm that these lower momentum I^{2+} ions arising from this pump-probe process do not contribute significantly to the correlations considered in the present work, we also present the I^{2+} momentum distribution from the two-fold (I^{2+}, C^+) covariance. As expected, we observe that only high-momentum (>200 a.u.) I^{2+} ions contribute to this signal. Consequently, we believe that the effect of the NIR laser is very

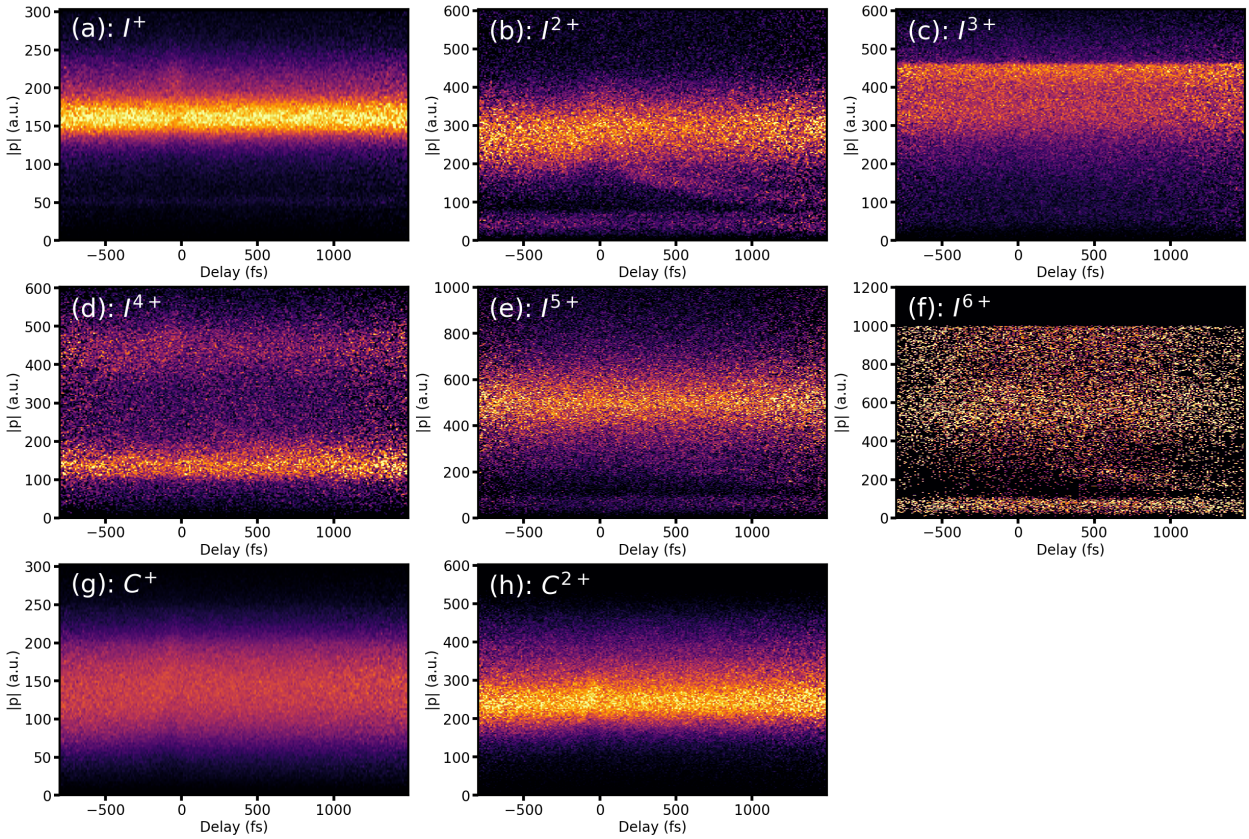

Figure S1: Different fragment's momentum distribution as function of pump-probe delay.

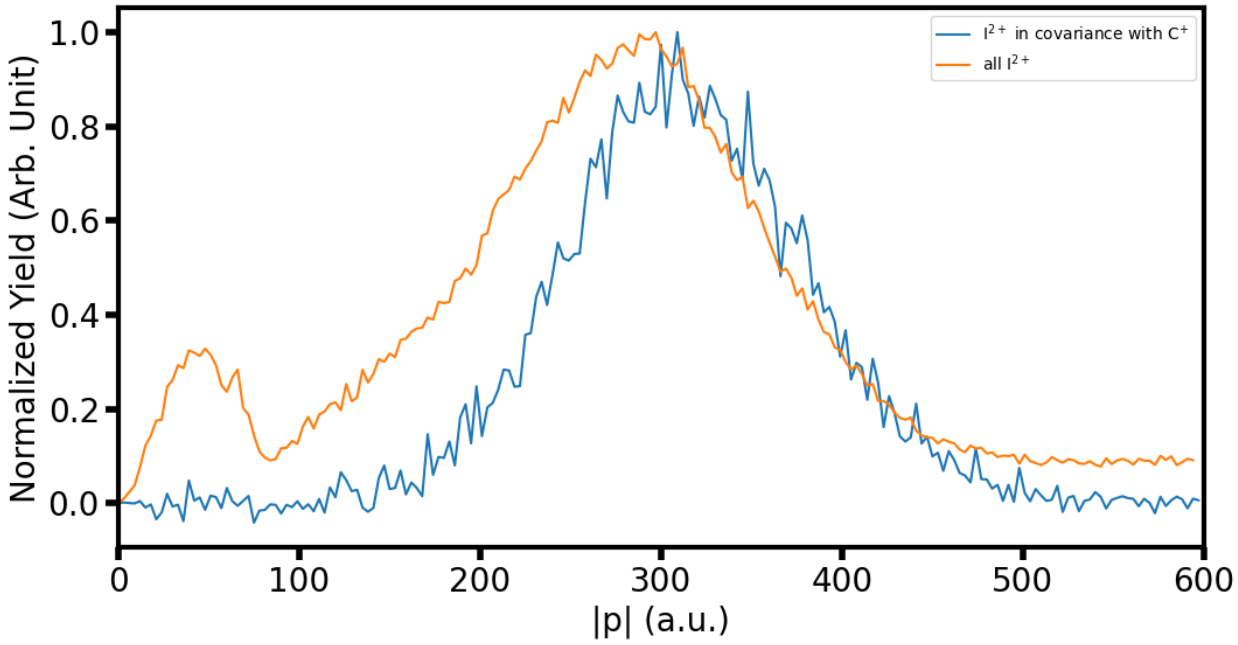

Figure S2: Comparison of I^{2+} fragments' momentum distribution of all counts and in covariance with C^+ fragment.

minimal on the data presented, which essentially only reflects the X-ray induced Coulomb explosion of ground-state C_4H_7I molecules.

Experimental data analysis and filtering

As outlined in the main text, we define the molecular frame in the following manner: the I^{2+} momentum is aligned along the $+p_x$ axis (purple arrow), while one reference C^+ is placed in the p_x–p_y plane ($p_y > 0$, $p_z = 0$). These choices define the I–C axis and a reference plane in the molecular frame. The resulting three-dimensional distributions of all carbon ions are presented in Figure S3(a)–(d). Here we compare different representations/analysis procedures of the experimental data.

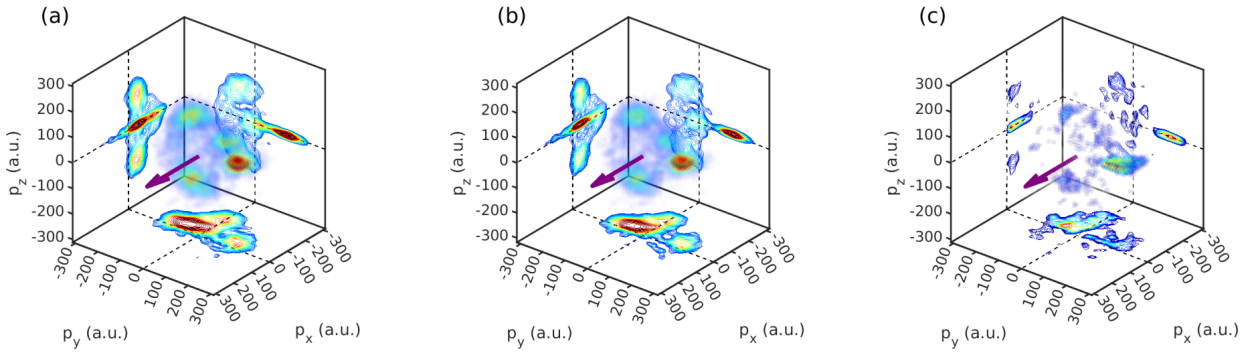

Figure S3: Molecular frame representation of 3-body channel (I^{2+}, C^+, C^+) with different methods (panels (a), (b)), as well as 4-body cumulant channel (I^{2+}, C^+, C^+, C^+) in panel (c).

Figure S3 (a) and (b) show the comparison between the unfiltered and filtered three-dimensional molecular-frame distributions for the (I^{2+}, C^+, C^+) channel. In the filtered case, when constructing the covariance histograms, we retain only events where the angle between the I^{2+} and the reference C^+ lies within 0–135°, thereby excluding configurations in which the central carbon is incorrectly assigned as the reference. From the plots, it is clear that the two distributions are in broad agreement. This arises because selecting a terminal carbon as the reference is three times more likely than selecting the central carbon. Thus, the filtering removes only one quarter of the events. Moreover, when the central C is selected as the reference, the molecular frame is poorly defined, leading to broadly-distributed signal across the molecular frame. As a result, removing events in which the central C is the reference does not significantly alter the overall distribution. Panel (c) shows the equivalent plot arising

from a 4-body cumulant analysis (I^{2+}, C^+, C^+, C^+), which exhibits lower statistics.

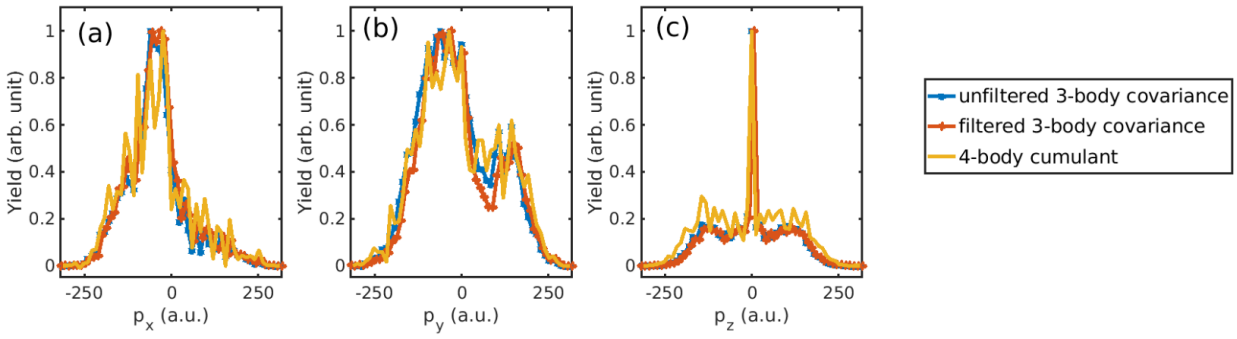

Figure S4: The 1D projections of molecular frames in Figure S3. (a)-(c) are the p_x, p_y and p_z projections of the three different distributions.

Figure S4 shows the 1D projections of the experimental relative momentum distributions along p_x, p_y and p_z axis (panels (a)-(c)) from the 3D distributions shown in in Figure S3 (a)-(d). Figure S4 demonstrates the effect of the aforementioned momentum filtering on the three-body covariance analysis, and how these compare to the four-fold cumulant analysis. The momentum filtering on the three-fold covariance has minimal effect in these 1D distributions, seemingly slightly increasing the distinction between features in the y dimension. The projection of the relative momentum distributions from four-fold cumulant analysis are very similar to those from the three-fold covariance analysis, albeit with a worse signal-to-noise ratio, as expected and discussed in the main text.

Coulomb Explosion Imaging Simulations

In order to better understand the contributions of the protons to the overall Coulomb explosion dynamics, we performed classical Coulomb explosion simulations with different number of charges on the hydrogen atoms, observing their influence on the final momentum of the heavy ions. Figure S5 presents the 2D projections of the recoil-frame C^+ momentum in the (I^{2+}, C^+, C^+) channel, assuming no charge on the hydrogen atoms (red, presented in the main text) and 1 charge on each hydrogen atom (blue). In each case, the pool of initial molecular geometries is sampled through Gaussian blurring in the same manner. The resulting distributions overlap almost perfectly, suggesting that, under the assumption of an instantaneous and classical Coulombic repulsion, the protons do not significantly influence the momentum of the heavier ions produced in a given explosion.

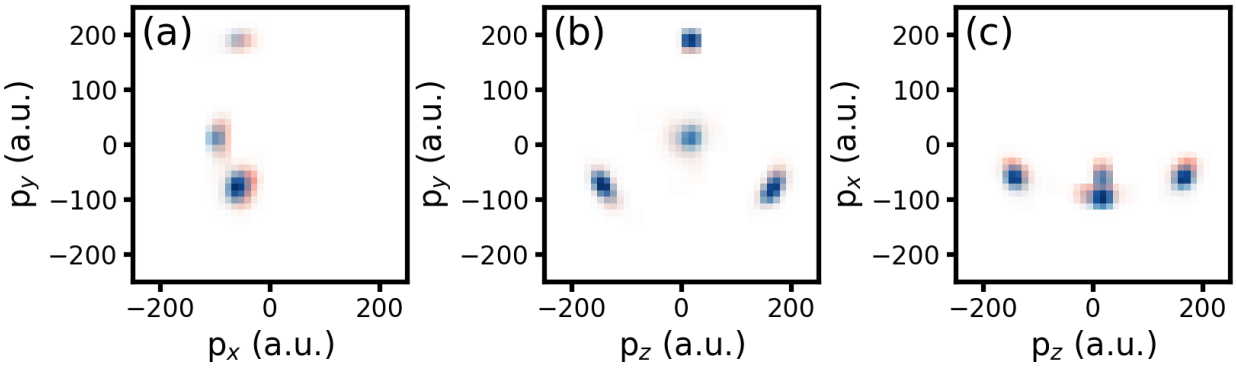

Figure S5: Comparison of the 2D projections of the C^+ momenta in the recoil frame for classical Coulomb explosion simulations in which all hydrogens are neutral (red) or singly charged (blue).

Finally, we turn to the influence of distorting the initial molecular geometry on the simulated relative momentum distributions. Figure S6 presents an extended version of Figure 4 in the main text, including the third symmetric motion, the I–C stretch, in Figure S6 to compare with the other two symmetric motions (I-C-C angle, C-C symmetric stretch). It is clear that this motion alone does not resolve the discrepancies with the experimental data. This is reasonable: if the central C is pushed toward the I atom, the resulting geometric response will likely involve changes in both the angle and the C–C bond lengths, thereby

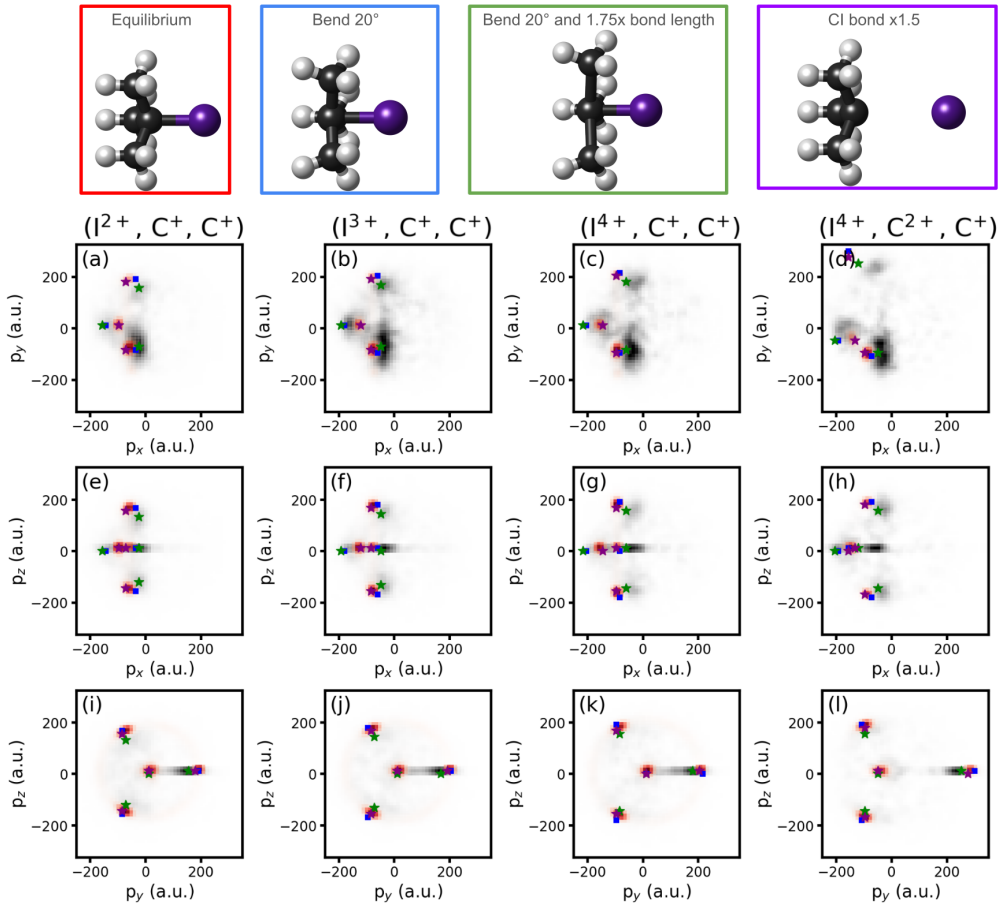

Figure S6: Extended version of Figure 4 in the main text. Three different motions C-I, I-C-C angle, C-C symmetric stretch are shown here. (a)-(l) are the $p_x - p_y$, $p_x - p_z$, $p_y - p_z$ projections of the four channels in the main text.

coupling into the other two modes. These latter modes have a larger impact on the final relative ion momentum distribution.

We can further explore the influence of these geometric distortions by changing the magnitude of the distortion along each of these motions. This is presented in Figure S7. It can be seen that changing the I-C-C angle (upper two rows) affects the lower total charge state channels more than that the higher total charge state channels. The C-I stretch (middle two rows) makes very little change to the final momentum of the terminal carbons but has a large influence on the momentum of the central C. It also has an influence on the (I^{4+}, C^{2+}, C^{+}) channel, where the charge is asymmetrically distributed. The C-C symmetric stretch (bottom two rows) affects the relative momentum distributions significantly, mostly in improving agreement with the experimental result. This does not lead to perfect agreement however, and for all magnitudes of changes some discrepancies remain in each channel. The above observations again suggest that the deviation of the experiment with the simple point charge model assuming an equilibrium geometry arises from complex multi-dimensional motions of the molecule during the charge build-up process (likely in addition to factors neglected by these simulations - such as deviations of polycationic potentials from purely Coulombic behavior).

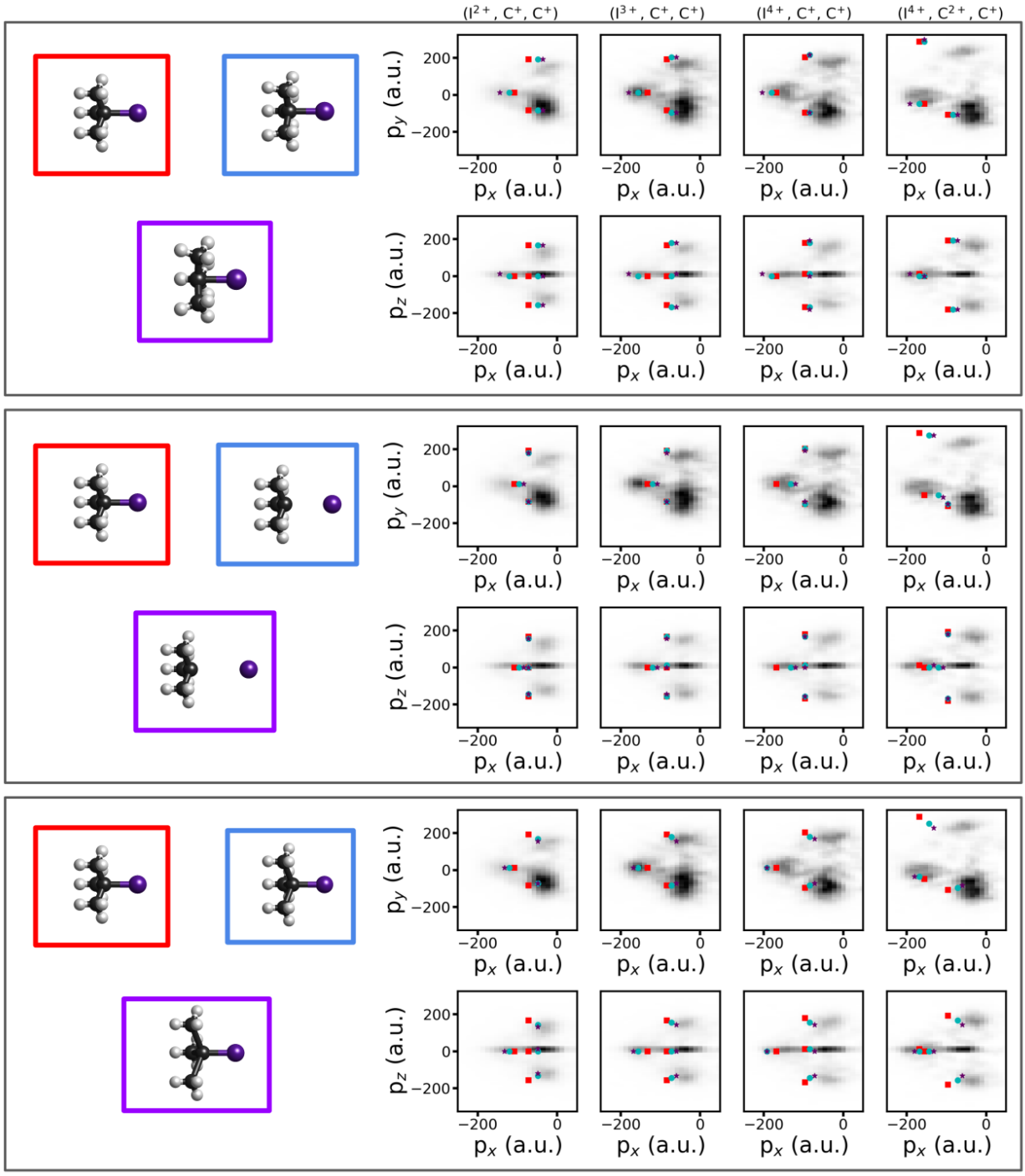

Figure S7: Three different motions (I-C-C angle, C-I, C-C symmetric stretch) are shown here. The first two rows are the $p_x - p_y$, $p_x - p_z$ projections for the four channels mentioned in the main text, overlaid with single geometry CEI simulation along I-C-C angle. The red square is no change. The cyan circle is a little change (-10 deg). The purple star is the biggest change (-20 deg). The middle two rows are the 1.40x (1.75x) C-I bond length motion. The bottom two rows are the 1.25x (1.50x) bond length C-C symmetric stretch motion.